


Article

Energetical and Exergetical Analyses of a Concentrating PV/T Collector: A Numerical Approach

Theodoros Papingiotis, Dimitrios N. Korres, Irene Koronaki * and Christos Tzivanidis 

School of Mechanical Engineering, National Technical University of Athens, 157 80 Athens, Greece; thpapingiotis@mail.ntua.gr (T.P.); korres@central.ntua.gr (D.N.K.); ctzivan@central.ntua.gr (C.T.)

* Correspondence: koronaki@central.ntua.gr

Abstract: The specific work presents an optical and thermal investigation of a hybrid thermo-photovoltaic solar collector with an asymmetrical compound parabolic mirror. Such collectors offer an innovative and sustainable approach to address both the thermal and electrical demands of residents on islands using renewable sources of energy and thus reducing the dependency on fossil fuels. The main goal of this investigation involves an analysis of the prementioned type of solar collector, incorporating an innovative and cost-effective numerical modelling technique aiming to enhance comprehension of its energy and exergy performance. The optical performance of the collector was calculated first with ray tracing for the month of June, and the ideal slope was determined for the same month. After the optical analysis, the energy and exergy performance were both estimated by implementing a novel numerical method in both COMSOL and SolidWorks. Based on the optical analysis, it was determined that the most favorable inclination angle for achieving optimum optical efficiency on the mean day of June is 10° . The thermal analysis, focusing on thermal efficiency, showed a maximum deviation of 5.3% between the two solutions, which indicates the reliability of the method. The collector achieved a maximum thermal efficiency of 58.55% and a maximum exergy efficiency of 16.94%.

Keywords: photovoltaic/thermal collector; numerical simulation; optical analysis; thermal analysis; exergy analysis



Citation: Papingiotis, T.; Korres, D.N.; Koronaki, I.; Tzivanidis, C. Energetical and Exergetical Analyses of a Concentrating PV/T Collector: A Numerical Approach. *Appl. Sci.* **2023**, *13*, 10669. <https://doi.org/10.3390/app131910669>

Academic Editor: Davide Astiaso Garcia

Received: 7 July 2023

Revised: 1 September 2023

Accepted: 22 September 2023

Published: 25 September 2023



Copyright: © 2023 by the authors. Licensee MDPI, Basel, Switzerland. This article is an open access article distributed under the terms and conditions of the Creative Commons Attribution (CC BY) license (<https://creativecommons.org/licenses/by/4.0/>).

1. Introduction

Photovoltaic thermal solar collectors have gained attraction in renewable energy systems, as they allow the conversion of solar radiation into both electrical and thermal energy. These collectors could be utilized for a variety of applications in the industrial and building sectors, such as the provision of domestic hot water (DHW) [1], air-conditioning [2], desalination [3], solar cooling [4], polygeneration systems [5] and industrial heat production [6–8]. The two main types of solar collectors are the concentrating and the non-concentrating collectors [9]. Collectors from both types have been examined numerically and experimentally, considering the thermal, the electrical and the optical operation.

The non-concentrating PV/T solar collectors have been studied and investigated in various studies in the literature. Sun et al. [10] created a mathematical model regarding the dynamic simulation of how a water system with a flat plane PV/T absorber works, which was verified with regards to its validity via indoors empirical data from experiments. They examined the slope effect and the effect of the collector's connection on the electrical and the thermal operation of this system, which was installed on a vertical façade in a building. They found that the type of connection for the solar PV/T had a greater impact on the thermal operation than on the electrical operation, and the optimum tilt angle was 40° . Kallio and Siroux [11] performed an exergetic and energetic study of a PV/T system in different locations and then optimized the design with regard to the exergy efficiencies. Rejeb et al. [12] established a numerical simulation model for the analysis of hybrid solar

collectors. With the developed model, they investigated the effect of a few parameters (solar radiation, water temperature at the inlet and the glazing covers number) on the collector's thermal operation performance. Moreover, they studied the monthly thermal and electrical operation of the collector considering the climatic conditions of Tunisia, where they found that the maximum electrical power was 8119 kWh/m² while the maximum thermal energy was 49,440 kWh/m². Lämmle et al. [13] researched the impact of low-emissivity coating, based on silver, on the electrical and thermal performance of a flat plane PV/T collector. A numerical model considering the energy balance was created and validated with results coming from experiments. The study shows that the coating reduced the heat losses by 8% with a minimal effect on the electric performance, compared with the same collector without the coating. Aste et al. [14] developed a simulation model for an uncovered PV/T collector which took into consideration the main parameters affecting the collector efficiency, a model which was also validated using empirical results. Kazem et al. [15] created a numerical model to investigate different geometries for the flow channels, which was then studied experimentally and compared to a conventional PV module. The main conclusion was that the spiral flow collector presented the highest electrical performance of 9.1%. Herrando et al. [16] performed a 3-dimensional computational fluid dynamics analysis (CFD) study on different absorber geometries. An absorber with rectangular channels achieved better thermal performance than the reference case of a commercial hybrid collector with flat elements.

While solar thermal concentrated collectors have been studied extensively [17,18], few works in the literature have been found that consider hybrid concentrated collectors. Bernardo et al. [19] proposed a methodology for the characterization, simulation and evaluation of a concentrated hybrid collector. Then, they applied it to a collector with a parabolic reflector and compared the results with conventional PV modules and a conventional solar collector. A dynamic theoretical model was developed by Karathanassis et al. [20] for the long-term performance evaluation of a concentrating thermo-photovoltaic collector with a parabolic mirror. The model validity was verified using data from experiments on a prototype system, and an exergetic optimization was performed. Rosell et al. [21] designed a concentrating hybrid system consisting of a Fresnel mirror with a channel PV/T collector which achieved a thermal performance of over 60%. An analytical model was also developed and validated based on the data produced. A PV/T element with a Fresnel mirror and a nanofluids-based optical filter was proposed by Wang et al. [22]. By using ray tracing through the Monte Carlo method, the overall optical performance was estimated to be 93.54%, while CFD analysis indicated 18.52% thermal efficiency. Nilsson et al. [23] experimentally examined the effect of different materials used for the construction of an asymmetric compound parabolic reflector. They constructed reflectors from anodized aluminum and aluminum steel (laminated). The analysis conducted showed no difference in the yearly output between the two materials. Koronaki and Nitsas [24] studied and observed the performance of five asymmetric PV/T solar collectors equipped with flat absorbers. The collectors were connected serially. A novel mathematical approach was created, and the respective results were compared with experimental data and validated. Nasserian et al. [25] created a two-dimensional CFD analysis of a hybrid asymmetric compound parabolic collector (ACPC). The model was then validated with experimental results, and the optimum tilt angle was determined for Gävle, Sweden. Several modifications, such as insulation for the back of the reflector and different material for the absorber, were studied.

The referenced sources make it evident that although there is a substantial body of work dedicated to examining solar collectors, the understanding of complete combined 3D optical and thermal simulations for asymmetrical concentrating hybrid solar collectors remains relatively constrained. Although previous studies indicate the existence of 3D simulations, this study offers a novel way to analyze these collectors and uses its results to create equations to describe their thermal behavior.

This paper presents a comprehensive analysis of an ACPC-PVT collector which is suitable for applications in islands, as it combines electricity and thermal energy production. The study encompasses several aspects, including an optical analysis based on the ray tracing approach of Monte Carlo, to determine the ideal angle of inclination for the solar unit to ensure maximum energy generation, as well as the development of a novel numerical modeling technique for the thermal simulation. The method was established through two simulating programs (COMSOL and SolidWorks), and the reliability of the method was verified by comparing the results produced by the prementioned tools. The energetic and the exergetic performance of the studied solar collector is presented and analyzed.

In summary, the objective of this work is to foster comprehension regarding the thermal performance of the ACPC-PVT collector, employing the outcomes of both the ray tracing analysis and the CFD simulations. The last ones employ a new methodology developed by the authors, in which the air inside the cavity is taken into consideration for the thermal simulation without including it in the computational domain, reducing the size of the mesh grid and consequently the computational cost of the analysis. By conducting the ray tracing analysis, a thorough comprehension of the limitations of the design is obtained. Meanwhile, by linking the findings from the CFD simulations to different inlet temperatures, the capacity to comprehend certain model outcomes without requiring a fresh complete CFD simulation on every occasion is provided.

2. Materials and Methods

2.1. Description of Solar Collector

An asymmetric compound parabolic collector with a double flat plate PV/T absorber was examined. The reflector's profile consists of a sequence of a circular and a parabolic line. The center of the circular part of the collector is equivalent to the parabola focal point.

The absorber material is aluminum and the heat transfer fluid flows through eight conduits of an elliptical cross section. PV cells are located on both the upper and the back side of the receiver. In total, there are 152 mono-crystalline-type cells divided into two identical strings, one for the absorber's upper side and one for the downside. A thin layer of silicone is placed between the receiver and the PV cells and on the exposed PV side. The collector is protected by a glass cover.

The main collector characteristics are summarized in Table 1. Moreover, Figures 1 and 2 present the examined collector.

Table 1. Collector characteristics [25].

General Characteristics	Value
Length of the collector	2290 mm
Width of the collector	464.52 mm
Width of the receiver	157 mm
Thickness of the aluminum hydroskeleton	6.50 mm
Thickness of the reflector	4.00 mm
Major radius of the elliptical channel	7.00 mm
Minor radius of the elliptical channel	1.75 mm
Radius of the circle	144.86 mm
Focal length of the parabola	144.86 mm
Concentration ratio	1.51
Thickness of the glass cover	4 mm
PV temperature dependence	−0.64%/K
PV nominal efficiency	18.7%

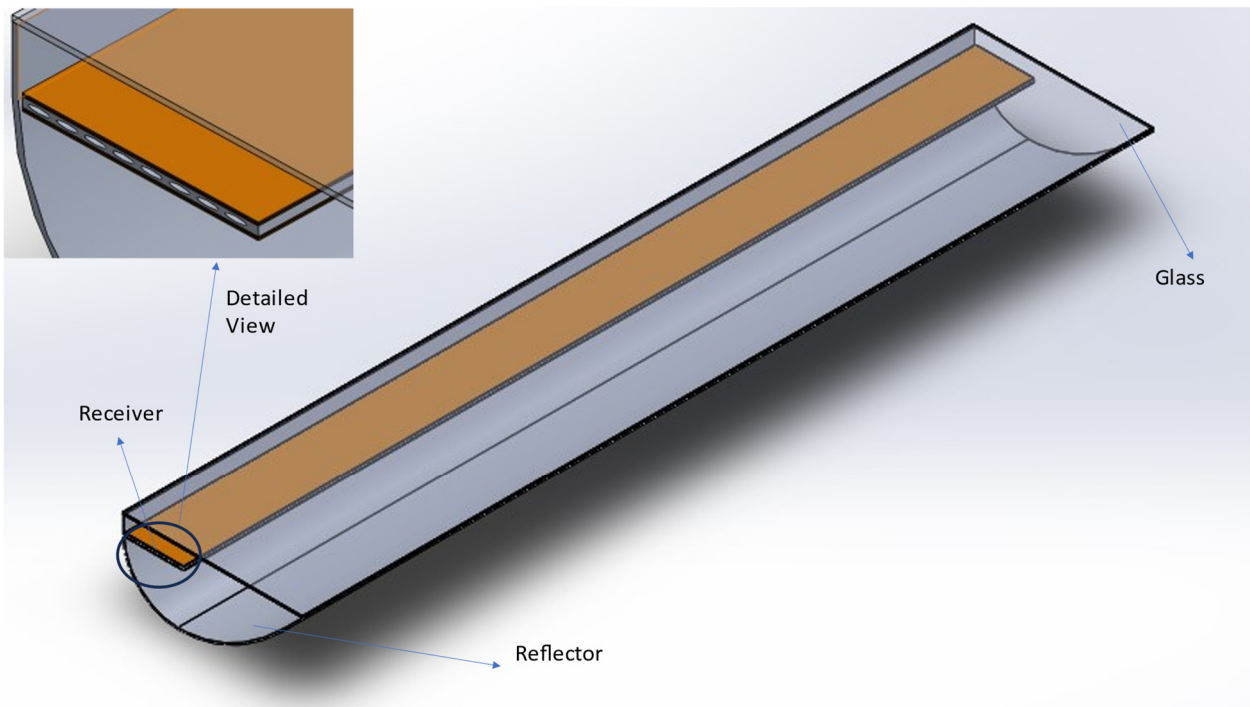


Figure 1. 3D view of the examined collector.

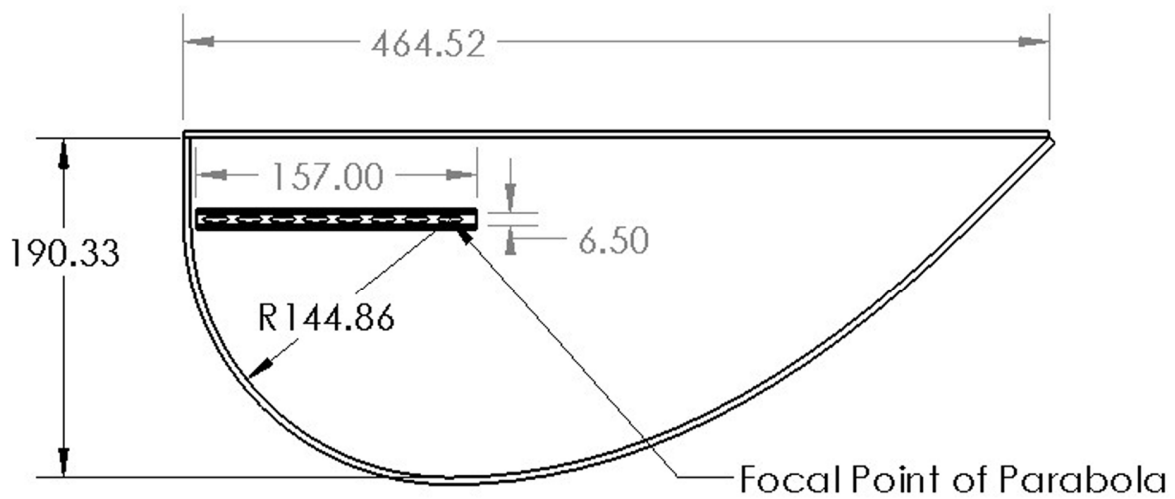


Figure 2. Primary dimensions of the solar unit.

The properties as regards the optical operation of the solar unit are presented in Table 2.

Table 2. Optical properties of the solar unit.

Optical Parameter	Values
Emittance of the cover	0.95
Emittance of the reflector	0.05
Emittance of the absorber	0.90
Reflectance of the absorber	0.94
Transmittance of the cover	0.95
Absorptance of the absorber	0.93

2.2. Mathematical Formulation

This subsection provides the formulations utilized for thermal and optical analyses. Firstly, the electrical efficiency in terms of electricity production is affected by the temperature of the PV cells, as it is described in Equation (1) [24,25].

$$\eta_{el} = \eta_0 \cdot (1 - \beta_c \cdot (T_{pv,m} - T_0)) \tag{1}$$

Another alternative way for the electrical efficiency calculation is given in Equation (2) [26].

$$\eta_{el} = \frac{Q_{el}}{G_{pv} \cdot A_{pv}} \tag{2}$$

In the above equation, η_0 represents the cell efficiency considering standard testing conditions (STCs) ($STC, G = 1000 \frac{W}{m^2}, T_0 = 25 \text{ }^\circ\text{C}$). β_c denotes the coefficient of temperature with regards to the photovoltaic (PV) module. A mean value for the PV was taken into consideration.

By combining Equations (1) and (2), the electrical production for the cells in the absorber upper side is calculated using Equation (3) [24].

$$Q_{el,up} = A_{pv,up} \cdot G_T \cdot \eta_0 \cdot (1 - \beta_c \cdot (T_{pv,up,m} - T_0)) \tag{3}$$

The available solar irradiance that reaches the absorber down side is calculated using Equation (4) [24].

$$G_{cpc} = G_T - \frac{1}{C} \cdot G_d \tag{4}$$

where G_d represents the intensity of diffuse radiation from the sun, G_T denotes the solar radiation that directly falls on the collector aperture perpendicularly and C represents the ratio of concentration, which indicates the ratio between the glass area and the area of the hybrid absorber [18].

$$C = \frac{A_g}{A_r} \tag{5}$$

As a result of the above equations, the electrical production of the cells located on the bottom side of the receiver is defined using Equation (6) [24].

$$Q_{el,down} = A_{pv,down} \cdot G_{cpc} \cdot \left(\frac{A_{pv,tot}}{A_{pv,down}} C - \frac{A_{pv,up}}{A_{pv,tot}} \right) \cdot \eta_0 \cdot (1 - \beta_c \cdot (T_{pv,down,m} - T_0)) \tag{6}$$

The effective solar radiation, which is perpendicularly oriented on the collector aperture, can be written using Equation (7) [18]:

$$G_{eff,T} = G_{b,T} + \frac{G_d}{C} \tag{7}$$

The efficiency in terms of thermal operation is determined using Equation (8) [27].

$$\eta_{th} = \frac{m \cdot Cp \cdot (T_{out} - T_{in})}{A_g \cdot G_{eff,T}} \tag{8}$$

where the numerator is the useful heat, which is defined by multiplying the mass flow rate of heat transfer fluid (m) with the specific heat capacity of the medium (Cp) and the difference between the outlet and inlet temperature ($T_{out} - T_{in}$). The denominator is the result of the surface area of the solar unit and the effective radiation of the sun, which is defined using Equation (7).

The sky temperature, as a function of the ambient temperature, is calculated using Equation (9) [28].

$$T_{sky} = 0.0552 \cdot T_a^{1.5} \tag{9}$$

Equation (10) is employed to determine the coefficient of the heat transfer between the outer collector surfaces and the surrounding air [25].

$$h_{wind} = \frac{8.6 \cdot u^{0.6}}{L^{0.4}} \quad (10)$$

The parameter u represents the velocity of the wind in meters per second (m/s), while L denotes the collector's length measured in meters (m).

Reynolds number is calculated using Equation (11) [18]:

$$Re = \frac{uD_h}{\nu} \quad (11)$$

Parameter u is the mean velocity of the water in the channel, ν is the kinematic viscosity and D_h represents the hydraulic diameter, which is expressed using Equation (12) [29]:

$$D_h = \frac{4A}{P} \quad (12)$$

Parameter A is the cross-sectional area of the channel and P is the channel perimeter. The mean fluid velocity is calculated with the following equation:

$$u = \frac{\dot{m}}{\rho \cdot A_h} \quad (13)$$

A_h is the cross section of the hydraulic diameter.

To ascertain if the flow appears to have turbulent or laminar characteristics, the critical value of Reynolds number is taken into account through Equation (14).

$$Re_c = 140 \cdot \sqrt{\frac{8}{f}} \quad (14)$$

The flow is considered laminar when the Reynolds number ratio between the critical and the normal values is lower than unit ($\frac{Re_c}{Re} < 1$).

The factor of friction in the flow (f) is determined through the following equation. The subsequent formula utilizes the pressure drop (ΔP), which is obtained from the computational fluid dynamics analysis conducted for each case.

$$f = \frac{\Delta P}{\frac{L}{D_h} \cdot \frac{1}{2} \cdot \rho \cdot u^2} \quad (15)$$

The flow regime was found to be laminar in all the examined operating points. Thus, Equation (16), which gives the theoretical values of the friction factor considering laminar flow conditions, was utilized for verifying the results of Equation (15) (numerical model) [18].

$$f = \frac{64}{Re} \quad (16)$$

Except for thermal efficiency, it is important to calculate the exergy efficiency of the collector, as exergy efficiency provides a comprehensive measure of the quality and effectiveness of energy conversion within the system. The expression for the gain of useful exergy from the collector, accounting for the drop of the pressure, can be represented by Equation (17), where $T_0 = 25 \text{ }^\circ\text{C}$ [30].

$$E_{col} = Q_u - m_f \cdot C_p \cdot T_0 \cdot \ln\left(\frac{T_{out}}{T_{in}}\right) - \frac{T_0 \cdot W_p}{T_{f,m}} \quad (17)$$

The solar radiation exergy can be determined using Equation (18), as this is provided in References [24,31] with the assumption that the temperature of the sun is equal to 5770 K [28].

$$E_{sol} = Q_{sol} \cdot \left[1 - \frac{4}{3} \left(\frac{T_0}{T_{sun}} \right) + \frac{1}{3} \left(\frac{T_0}{T_{sun}} \right)^4 \right] \quad (18)$$

Assuming that the electrical production is useful exergy [24], the collector exergy performance is calculated using Equation (19) [24].

$$\eta_{ex} = \frac{E_{col} + Q_{el}}{E_{sol}} \quad (19)$$

Finally, the optical efficiency is calculated using Equation (20).

$$n_{opt} = \frac{Q_{abs}}{A_g \cdot G_{eff,n}} \quad (20)$$

Parameter $G_{eff,n}$ refers to the amount of solar radiation received on a surface that is perpendicular to the direction of the rays of the sun.

2.3. Numerical Modeling

2.3.1. Optical Analysis Details

An optical analysis based on the Monte Carlo ray tracing method was conducted in this study. This analysis was implemented by using Tonatiuh. Tonatiuh is a free and open-source program designed by the National Renewable Energies Center (CENER) that employs Monte Carlo ray tracing methods for simulating concentrating collectors. The software's findings were verified by comparing them with empirical data from various solar installations [32]. Additionally, it has been employed in several scientific articles examining the performance analysis of solar thermal collectors [33,34].

The analysis was performed using a sufficient number of rays, specifically 10^6 , which was determined after conducting a preliminary analysis while maintaining a constant direct solar irradiation of 1000 W/m^2 .

In the simulation, the collector was positioned in a southerly direction in the area of Athens, Greece, with the latitude and longitude parameters configured as 37.98° and 23.93° , correspondingly. Tonatiuh's internal libraries were utilized to compute the sun's position and determine the resulting orientation of the incident direct irradiation. These libraries considered time, date and coordinates as inputs.

2.3.2. Thermal Simulation Details

The thermal simulations in this study were performed using SolidWorks v.2014–2015 and COMSOL 5.2 software [35,36]. Both of these tools are widely used, with proven validity and reliability [18,27,37].

SolidWorks is a well-established simulation software extensively employed in various research studies focusing on energy systems, particularly in the context of solar thermal collectors [28,30]. This program facilitates design processes and allows separate or simultaneous simulations of flow, optical and thermal characteristics.

COMSOL is a readily available software that applies finite element methods for solving multi-coupled physics problems. COMSOL is a software tool employed in research studies concerning both non-concentrating [16,38] and concentrating solar collectors [39].

The authors developed a novel method for the thermal simulation that was applied in this study. The innovative aspect of this method stems from its consideration of the enclosed air between the reflector and glass while excluding it from the numerical simulation, leading to substantial reductions in computational time. Specifically, the simulated inclusion of enclosed air was accomplished by imposing boundary conditions that specified the temperature and equivalent value of the convective coefficient (h) on the absorber boundary

areas, as well as on the interior surfaces of the cover and reflector. Several simulations were carried out, varying the enclosed air temperature while keeping the convective heat transfer coefficient constant in each simulation. The purpose was to determine the appropriate value of the enclosed air temperature that would result in the heat losses that come from the absorber being similar to those from the external faces of the solar unit. This condition ensured that the solution would converge at each operational state, as the thermal equilibrium of the solar unit needed both losses to be equivalent. The total thermal losses were accurately calculated by considering both the radiative and convective contributions.

In the beginning, an arbitrary temperature value within the range of the inlet fluid temperature and the ambient air temperature was assigned to all the surfaces within the cavity to compute heat losses due to convection. Once the numerical solution was obtained, the total thermal losses from the absorber and the corresponding losses from the external faces of the solar unit were established. In the event that the receiver’s thermal losses exceeded those of the exterior surfaces, a greater temperature rate was assigned to the air gap. Increasing this temperature led to a decrease in overall losses for the receiver while causing the outer surfaces to reach higher temperatures, increasing their overall losses. This iterative process was repeated until an equilibrium was achieved.

This method was implemented for a subset of the examined operating points, revealing that it yields results that are comparable to those obtained by linearly interpolating between two observation points, with a 1 K variance in the temperature estimated within the air cavity.

In order to illustrate the step-by-step implementation of the proposed method, a flowchart has been developed (Figure 3). The flowchart visually captures the sequence of actions and decisions involved in each phase of the method. By referring to this flowchart alongside the following textual description, a holistic understanding of the analysis of the thermal performance of the ACPC-PVT collector can be obtained.

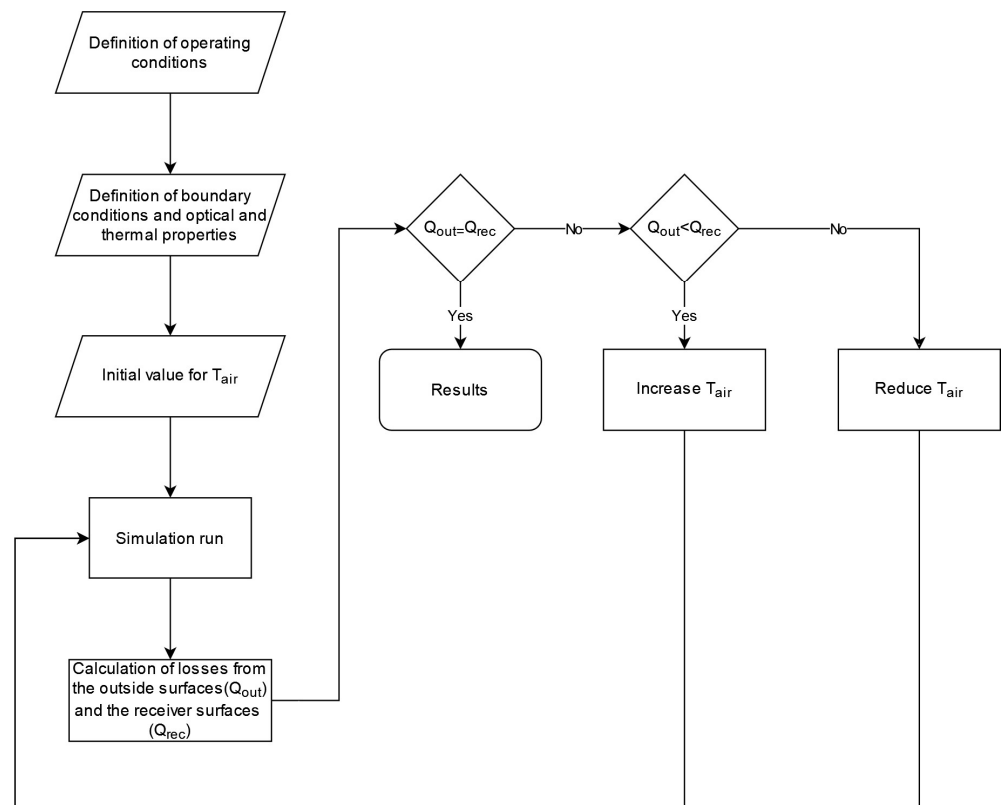


Figure 3. Flowchart of the proposed method.

Regarding the overall chosen solution approach, it should be noted that steady-state analysis was employed during the thermal analysis. This selection was deliberate, as the study aims to mainly investigate the inlet temperature increment impact on the thermal and exergy efficiency. Furthermore, the assumption of laminar flow as the flow regime was made. This assumption is consistent with reference [25], in which identical flow rate was employed for the experiments.

2.3.3. Mesh Information

In the present study, great attention was paid to the mesh grid formation, with several refinements taking place in order to ensure reliable results. This was attended to in both the COMSOL and SolidWorks models.

Specifically, the mesh along the boundaries between the fluid and the conduit surfaces underwent refinement, and the mesh elements used for the water were carefully adjusted and improved in order to better represent and simulate the thermal exchange involving the fluid and the receiver walls. Additionally, the mesh elements on the mirror and absorbing surfaces were fine-tuned to prevent issues related to absorption of solar irradiation and to enable effective ray tracing. By implementing this enhancement on the reflector, the interactions between the surfaces and the rays of light can be calculated with greater accuracy, providing better representation of the optical behavior of the collector in the simulation.

2.3.4. Boundary Conditions of Thermal Analysis

The parametric thermal investigation was conducted at the solar time of 12:00 for an average day of June. Based on the optical analysis for the solar unit at that specific moment and date, a slope angle of 10 degrees was identified as the optimum for the installation of the collector. This angle was implemented in the numerical modeling.

The solar irradiation values were acquired from the PVGIS [40], whereas the environment conditions and especially the external temperature and wind speed for the average day in June were sourced via Greece's Technical Chamber [41]. Based on these values and using Equation (10), the convective coefficient of the outer air on the outer surfaces was computed. As stated in Section 2.3.2, the coefficient took a constant value of $5 \text{ W/m}^2/\text{K}$, which is deemed appropriate for such enclosed spaces. Comparable values are documented in relevant studies [30,42].

The hybrid collector was investigated across a range of water temperatures at the inlet from $20 \text{ }^\circ\text{C}$ to $80 \text{ }^\circ\text{C}$, while the flow rate was kept constant at 2.2 lt/min . The selection of these values was based on their suitability for the specific application, as shown in reference [25].

The thermal boundary conditions are presented in Table 3.

Table 3. Thermal simulation operating conditions.

Parameter	Value
Outer air temperature ($^\circ\text{C}$)	26.5
Outer air speed (m/s)	3.3
Heat convective coefficient with ambient ($\text{W/m}^2/\text{K}$)	12.59
Heat convective coefficient with air in the gap ($\text{W/m}^2/\text{K}$)	5
Solar irradiance—direct (W/m^2)	725
Solar irradiance—diffusive (W/m^2)	218
Flow rate—volumetric (lt/min)	2.2
Inlet water temperature ($^\circ\text{C}$)	20–80

3. Results and Discussion

In the present section, the results of this study are provided with detailed analysis. Firstly, Figure 4 depicts the optical efficiency of the collector for the mean day of June. An hourly analysis was performed to determine the optimum value for the collector slope, as described in Section 2.3.1. The presented findings exclusively pertain to the morning

period, with the understanding that the same outcomes apply to hours beyond 12:00. To illustrate, the optimal inclination angle for 13:00 corresponds to that of 11:00.

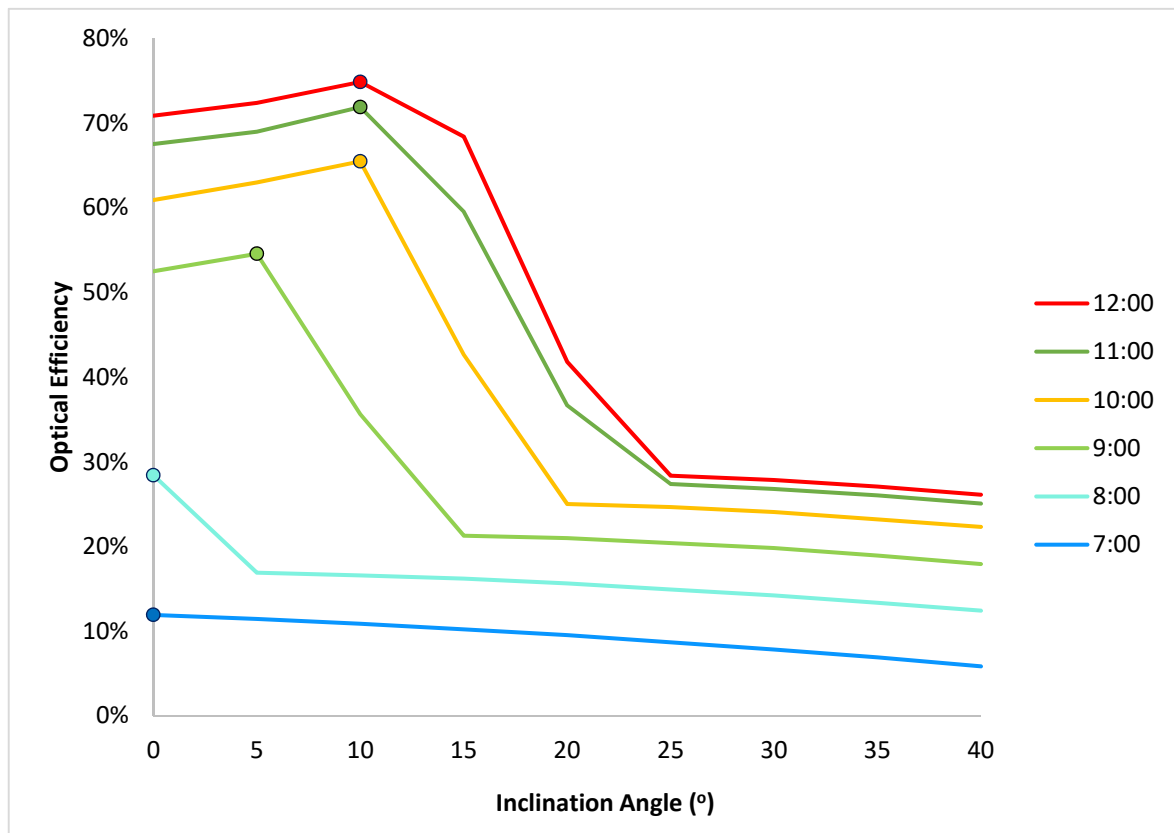


Figure 4. Optical efficiency of the solar unit for the mean day of June.

It is noteworthy that the optical efficiency of the solar collector is low in the early mornings and in the late afternoon period. Furthermore, sudden shifts in the performance of the collector are observed, especially for higher inclination angles. This phenomenon arises from the fact that, during these circumstances, the reflector does not contribute to solar utilization, leading to a drastic and abrupt reduction in the collector's useful reflective area. In addition, Figure 4 shows that a time period exists around the solar noon in which the optimal angle of inclination remains 10° . The maximum value of the calculated optical efficiency is 75%.

It is also remarkable to notice that the optical efficiency curves seem to be parallel to certain slope ranges which are different in each time moment, and that happens because in these ranges, the concentrator of the collector does not contribute to the solar energy utilization. Hence, in these cases, only the upper part of the receiver remains active for the solar energy absorption.

After establishing the optimal inclination angle based on Figure 4, the investigated solar unit was subjected to an analysis involving different inlet temperatures. This analysis aimed to evaluate the unit's performance under various operational conditions, specifically for the determined tilt angle.

Firstly, so as to verify the results from the simulation model, the Darcy friction factor was calculated. The Darcy friction factor was determined by comparing values obtained from the simulation and the theoretical calculations. The theoretical values were derived using Equation (16), whereas the numerical analysis utilized the pressure drop generated during the simulation by Equation (15). The values from the prementioned analysis are presented in Figure 5. A maximum deviation of 2.5% is observed. Therefore, the findings from the numerical analysis demonstrate close agreement with the theoretical values, affirming the reliability of the developed simulation model.

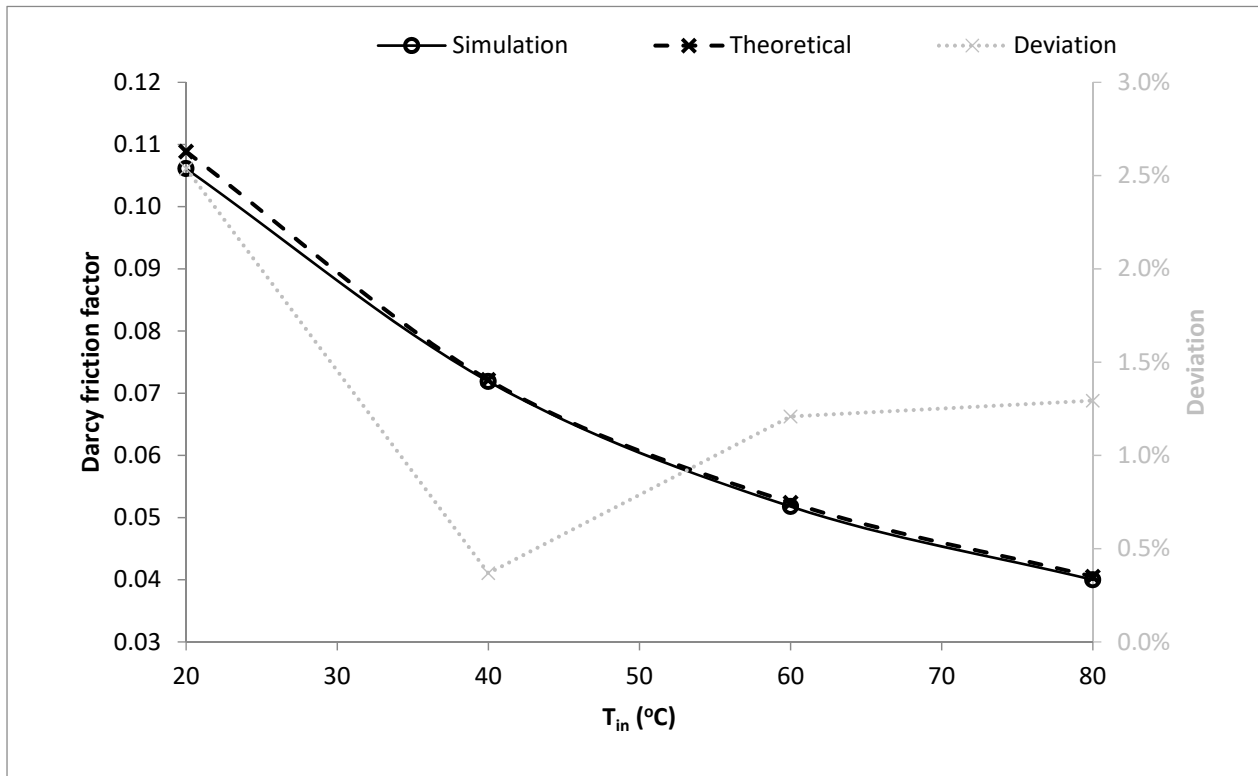


Figure 5. Darcy friction factor: numerical and theoretical values and their deviation with regards to inlet temperature.

Figure 6 illustrates the thermal solar collector performance, determined by applying Equation (8) and utilizing data from the two simulation tools employed. The obtained results demonstrate a strong correspondence between the two types of software, with a maximum deviation of 5.3% to be observed. These findings confirm the reliability and validity of the simulation method employed regarding the thermal modeling. The thermal performance line shows a downward trend with an increase in the water temperature at the inlet. This is a logical outcome because a higher temperature at the inlet results in greater losses, ultimately leading to a decrease in thermal efficiency.

Figure 7 showcases the temperature profiles of both the upper and the lower photovoltaic components, calculated using the simulation tools. Additionally, it presents the deviation between the two tools in each set of results. The temperature values are displayed as temperature differences relative to the inlet temperature, as this qualitative representation is more informative than quantitative values for visual analysis.

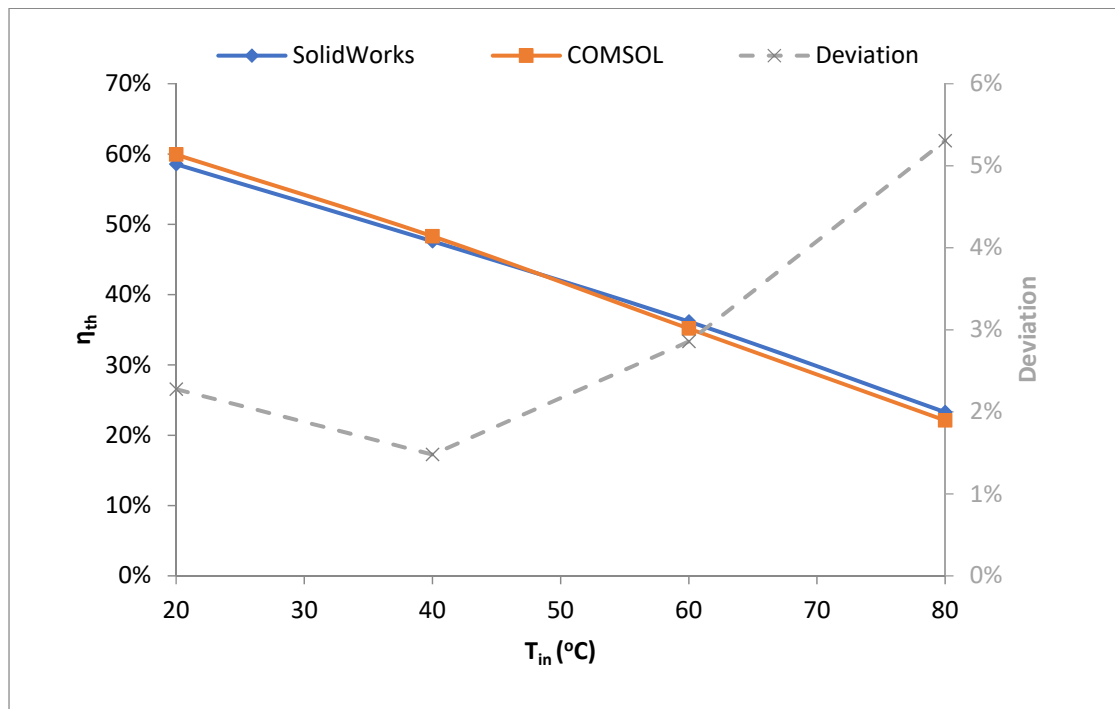
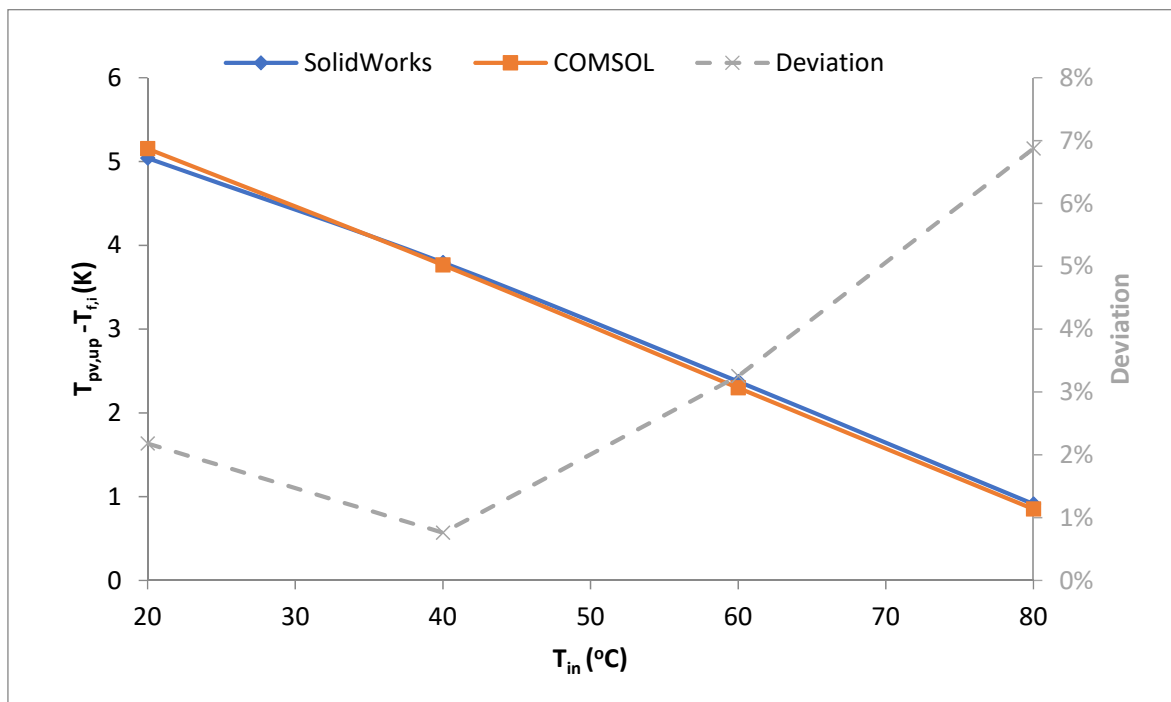


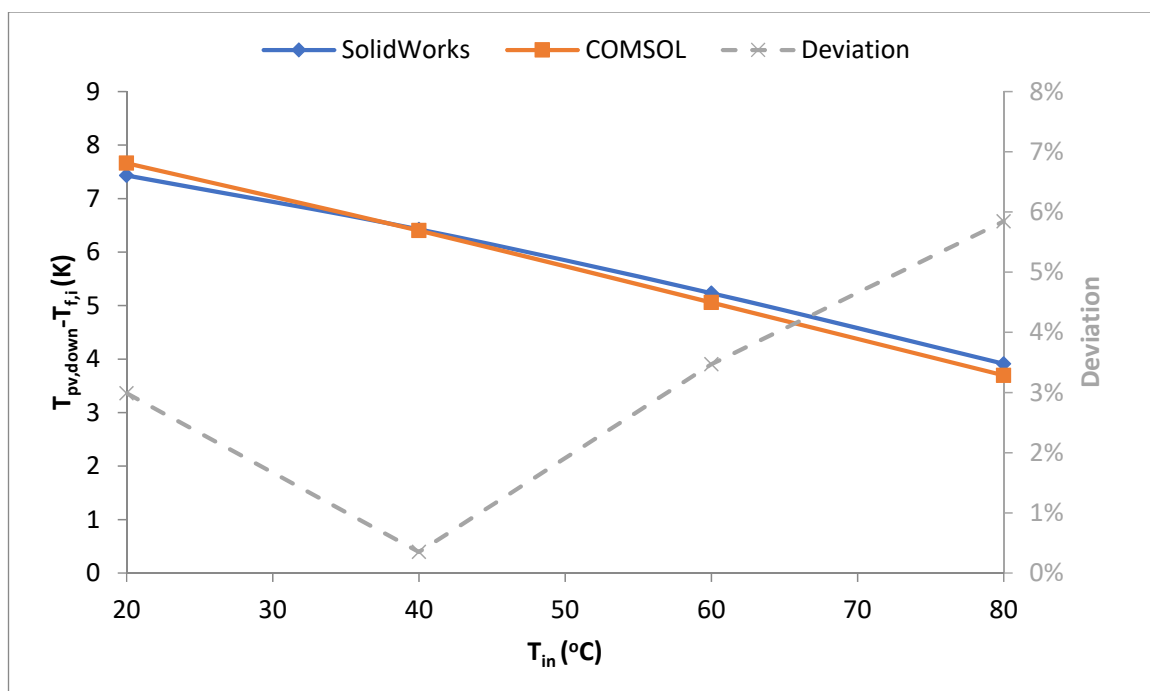
Figure 6. Thermal efficiency of ACPC-PVT: COMSOL and SolidWorks.

In particular, the results in Figure 7 exhibit a remarkably close agreement between SolidWorks and COMSOL results. Also, it is demonstrated that the calculated temperature profiles for both the upper and the lower photovoltaic components are highly similar. The maximum deviation of 6.87% between the two tools highlights the consistency and accuracy of the simulations. This close correspondence leads further credibility to the reliability of the simulation tools employed in this study.

From comparing Figure 7a with Figure 7b, it seems that the PV located on the lower part of the receiver consistently presents higher temperatures than the PV on the upper part throughout the entire range of operation. This observation can be attributed to the fact that the PV on the back side of the receiver receives a greater amount of solar irradiation. This discrepancy arises, also, because the solar radiation is focused in a narrower zone for the lower PV compared to the upper one, leading to higher temperatures, especially near the focal point. An intriguing observation is that the temperature delta involving the photovoltaic (PV) component and the temperature at the inlet tends to be larger at lower inlet temperatures. This happens because the convective regime inside the channels is being enhanced with the increment of the temperature at the inlet. Another purpose for this fact is that when the collector becomes warmer, it grows closer to the stagnation conditions in which the temperature fields converge with each other. Figure 8 further illustrates the above analysis by displaying the temperature allocation on the top and bottom PV. As described previously, the figure shows that as the working fluid warms up, a corresponding temperature rise is observed on the upper PV panel. Also, the focal point of the concentrator on the bottom side of the receiver is evident in the region characterized by the highest temperature at one end of the receiver.



(a)



(b)

Figure 7. Temperature delta of the (a) upper and (b) the lower PV by the inlet temperature.

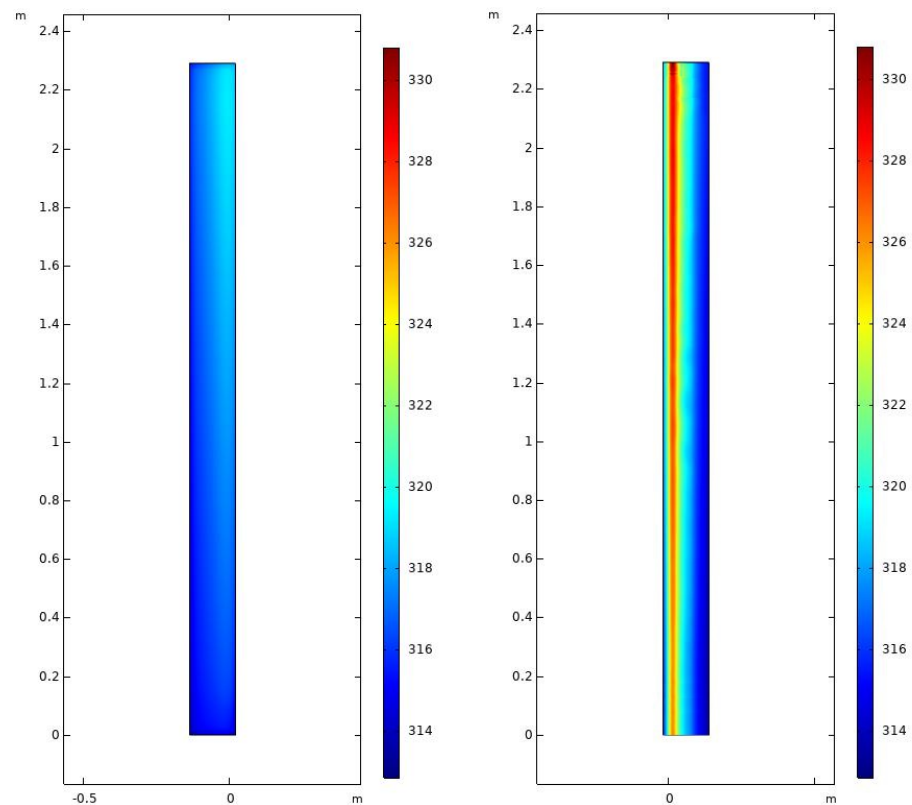


Figure 8. Temperature profiles at the top (left) and the bottom (right) PV of the receiver for $T_{f,i} = 40\text{ }^\circ\text{C}$.

Figure 9 visually represents the temperature difference between the ambient and the enclosed to the gap air, resulting from the procedure outlined in Section 4. Furthermore, Figure 9 clearly demonstrates the close agreement between the two numerical models, with a maximum deviation of 5.36%. The negative values are explained, since for the low inlet temperatures, the enclosed air temperature is lower than the ambient one.

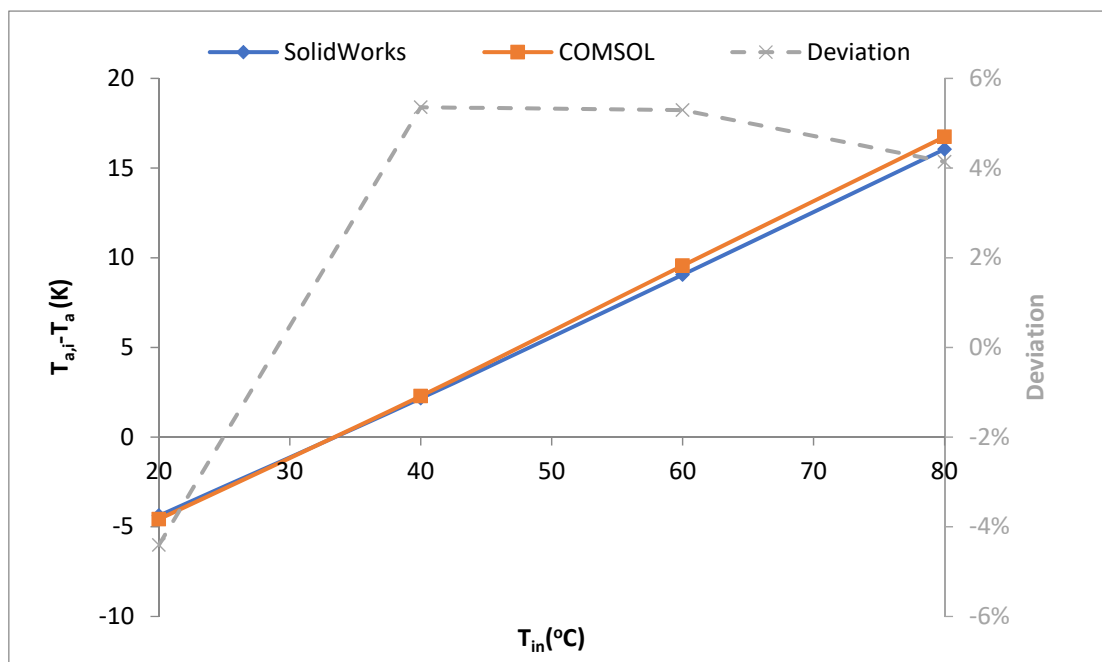


Figure 9. Temperature of the air in the gap with temperature on the inlet.

Figure 10 presents the air temperature within the collector's gap, as well as the temperatures of the receiver and the outlet. The objective is to assess the influence of the receiver and the outgoing temperature on the air temperature, as well as to observe the behavior of each one with respect to the rest temperatures.

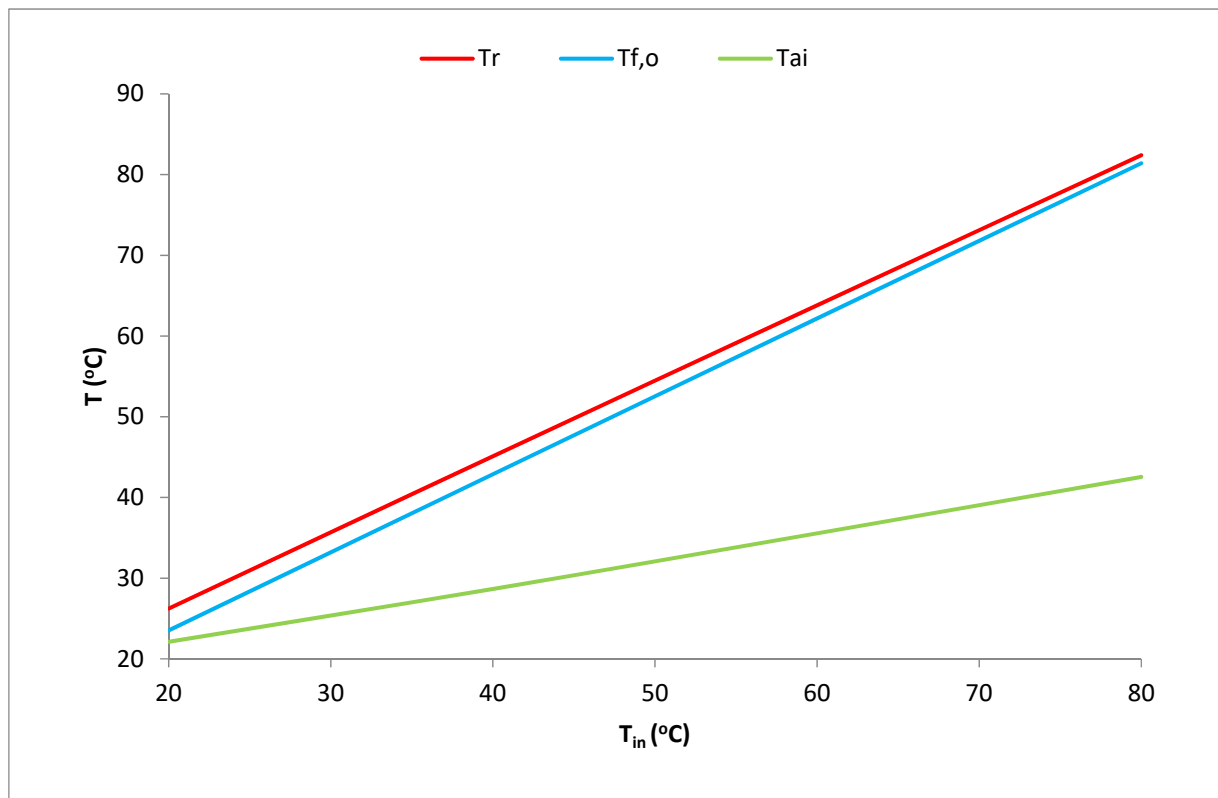


Figure 10. Absorber temperature, air in the gap temperature and outlet temperature.

According to Figure 10, the increment of the absorber temperature and the corresponding temperature at the outlet leads to the increment of the enclosed air temperature. However, this increment happens at a lower rate since the enclosed air has contact with the “cold” cover. Additionally, the temperature delta between the absorber and the fluid highlights that the temperature on the absorber tends to converge towards the water temperature as the temperature at the inlet rises, resulting in a decrease in the useful heat gained at a system level. The same trend was observed with the PV and water temperature in Figure 7, which is due to increase in the convection in the heat transfer process.

Figure 11 illustrates that the upper photovoltaic (PV) component exhibits higher efficiency compared to the lower PV. This can be attributed to the lower temperature developed in the upper PV, as presented in Figure 7. The temperature difference between the two PV components directly affects their performance, with the upper PV having up to 1.6% higher efficiency than the lower one.

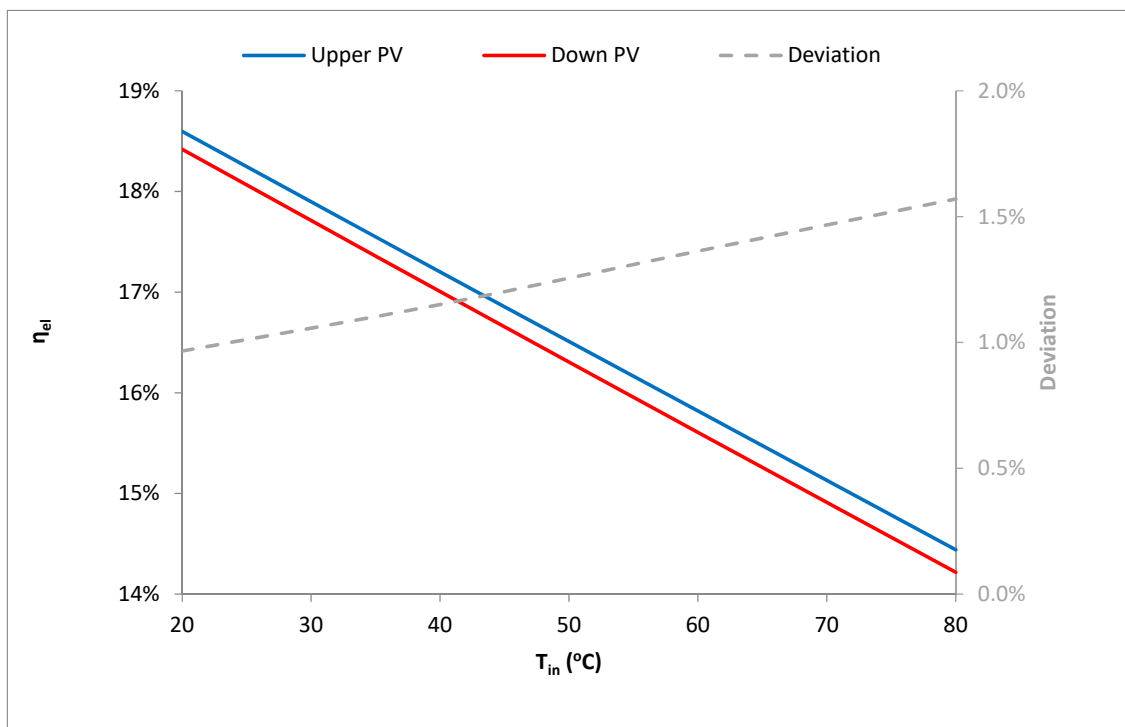


Figure 11. Electrical efficiency of the upper and lower PV with regards to inlet temperature.

Figure 12 shows the collector thermal and exergy efficiency as far as examined conditions are concerned. The efficiency in terms of thermal operation reaches a maximum value of 58.55% for the lowest temperature at the inlet, while the exergy efficiency takes the maximum value of 16.94% for 60 °C temperature at the inlet, which shows the optimum condition for the operation of the collector. It is remarkable to mention that operation around 60 °C is ideal both for hot water applications and for the PV efficiency.

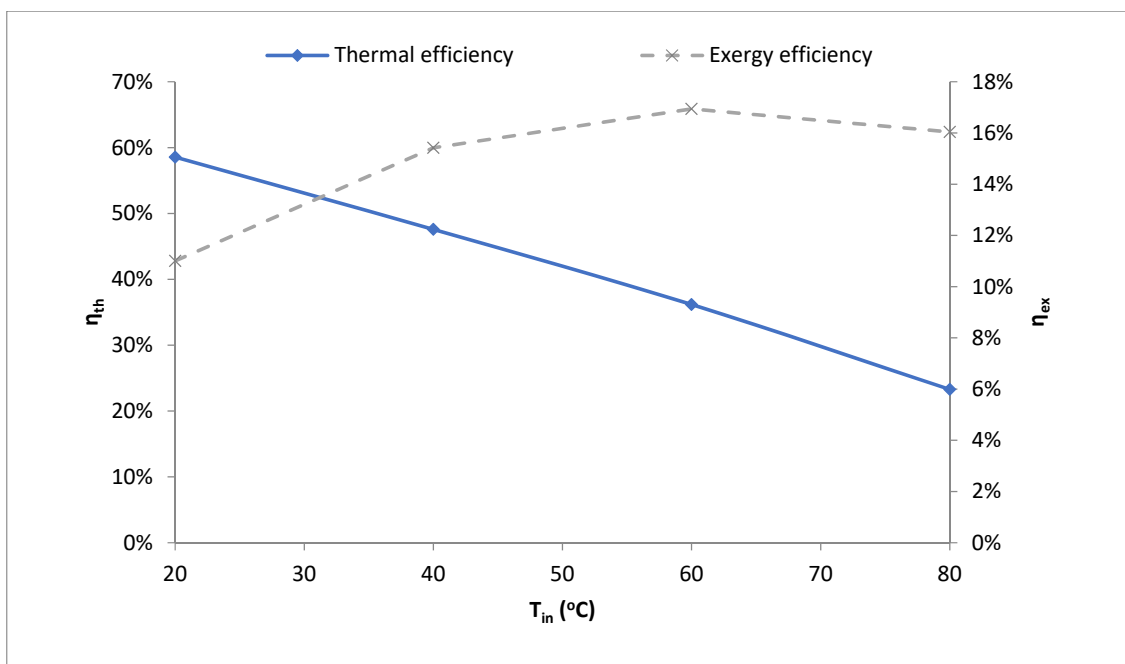


Figure 12. Exergetic and energetic efficiency of the solar unit.

Both the thermal and the exergy efficiency curves are approximated using the following polynomial expressions (second order) with a fitness factor of 99.86%.

$$\eta_{th} = -0.0000120 \cdot T_{in}^2 - 0.0046586 \cdot T_{in} + 0.6830038 \quad (21)$$

$$\eta_{ex} = -0.0000332 \cdot T_{in}^2 - 0.0041515 \cdot T_{in} + 0.0405358 \quad (22)$$

4. Conclusions

This research work investigated a PV/T collector with an asymmetric reflector, focusing on the optical and thermal performance. The outcomes of this study demonstrate how the proposed method for the computational model, which ensures low computational time, effectively portrays the behavior of the examined solar collector across various operating conditions, facilitating a deeper understanding of its energy and exergy performance. The primary outcomes of this paper are the following:

- For the average day of June, the optimal inclination angle to achieve the maximum optical efficiency (75% at solar noon) is 10°, as calculated through the optical analysis.
- The optimum angle of 10° ensures maximum values of the optical efficiency for four consecutive hours around solar noon, which is a remarkable time range.
- A mean value for the air temperature inside the collector was used to reduce computational time while achieving the necessary accuracy of the simulation.
- The collector thermal performance was examined and successfully verified through two simulation tools, SolidWorks and COMSOL. The mean deviation for the thermal efficiency was 5.3%.
- The applied simulation's validity was also verified by utilizing the Darcy friction factor. In particular, it was revealed that there was a deviation lower than 3.0% between the numerical simulation output and the values from the theoretical model.
- The electrical efficiency was reduced from approximately 19% to 14% when going to greater inlet temperatures. The upper PV efficiency was revealed to exceed the lower PV one by up to 1.6% because of the lower fields of temperature on the upper PV.
- The solar unit presents a maximum performance of 58.55% in thermal operation.
- The maximum efficiency in terms of exergy was found to take the value of 16.94%, which indicates that there is an optimum operating point for the particular collector regarding the examined month and the applied operating conditions.

Author Contributions: Conceptualization, T.P. and D.N.K.; methodology, T.P. and D.N.K.; software, T.P. and D.N.K.; validation, T.P. and D.N.K.; formal analysis, T.P. and D.N.K.; investigation, T.P. and D.N.K.; resources, I.K. and C.T.; writing—original draft preparation, T.P. and D.N.K.; writing—review and editing, I.K. and C.T.; visualization, T.P. and D.N.K.; supervision, I.K. and C.T.; project administration, I.K. and C.T. All authors have read and agreed to the published version of the manuscript.

Funding: The second author (D. N. Korres) would like to thank the Bodossaki Foundation for its financial support in his post-doctoral research. The duration of the particular scholarship is 3 years (01/09/2021-31/08/2024).

Institutional Review Board Statement: Not applicable.

Informed Consent Statement: Not applicable.

Data Availability Statement: Available after request.

Acknowledgments: The second author (D. N. Korres) would like to thank Bodossaki Foundation for providing him with a post-doctoral scholarship. This work is dedicated in memoriam of Konstantinos Korres, who was a milestone for the second author (D. N. Korres).

Conflicts of Interest: The authors declare no conflict of interest.

Nomenclature

General Parameter

A	Area, m ²
C _p	Specific heat capacity of the fluid, kJ/(kg K)
C	Concentration ratio, -
D	Diameter, m
E	Exergy flow, W
f	Friction factor, -
G	Intensity of solar radiation, W/m ²
h	Coefficient of heat convection, W/(m ² K)
L	Length, m
m	Mass flow rate, kg/s
P	Power, W
P	Perimeter, m
Q	Energy rate, W
Re	Reynolds number, -
Re _{cr}	Critical Reynolds number, -
T	Temperature, °C
u	Wind speed, m/s
V	Volume flow rate, m ³ /s
W	Power, W

Greek symbols

β	Coefficient temperature for PV element, %/K
ΔP	Pressure drop, Pa
η _{el}	Electric efficiency, -
η _{ex}	Exergy efficiency, -
η _{th}	Thermal efficiency, -
η _{opt}	Optical efficiency, -
ν	Kinematic viscosity, m ² /s
ρ	Density, kg/m ³

Subscripts

a	Ambient
abs	Absorbed
b	Beam
col	Collector
cpc	Utilized by the reflector
d	Diffuse
down	Bottom
eff	Effective
el	Electrical
g	Glass
h	Hydraulic
in	Inlet
m	Mean
n	Normal
opt	Optical
out	Outlet
pv	Photovoltaic
r	Receiver
ref	Reference
s	Solar
sky	Sky
sol	solar
sun	Sun
T	Perpendicular to aperture

th	Thermal
tot	Total
u	Useful
up	Top
wind	Wind
a	Ambient
0	Reference
Abbreviations	
ACPC	Asymmetrical compound parabolic collector
CFD	Computational fluid dynamics
DHW	Domestic hot water
PV/T	Thermo-photovoltaic
STC	Standard testing conditions

References

- Roshanzadeh, B.; Premer, L.R.; Mohan, G. Developing an Advanced PVT System for Sustainable Domestic Hot Water Supply. *Energies* **2022**, *15*, 2346. [\[CrossRef\]](#)
- Al-Alili, A.; Hwang, Y.; Radermacher, R.; Kubo, I. A High Efficiency Solar Air Conditioner Using Concentrating Photovoltaic/Thermal Collectors. *Appl. Energy* **2012**, *93*, 138–147. [\[CrossRef\]](#)
- Mittelman, G.; Kribus, A.; Mouchtar, O.; Dayan, A. Water Desalination with Concentrating Photovoltaic/Thermal (CPVT) Systems. *Sol. Energy* **2009**, *83*, 1322–1334. [\[CrossRef\]](#)
- Nitsas, M.T.; Papoutsis, E.G.; Koronaki, I.P. Experimental Performance Evaluation of an Integrated Solar-Driven Adsorption System in Terms of Thermal Storage and Cooling Capacity. *Energies* **2020**, *13*, 5931. [\[CrossRef\]](#)
- Calise, F.; d’Accadia, M.; Piacentino, A.; Vicidomini, M. Thermoeconomic Optimization of a Renewable Polygeneration System Serving a Small Isolated Community. *Energies* **2015**, *8*, 995–1024. [\[CrossRef\]](#)
- Herrando, M.; Simón, R.; Guedea, I.; Fueyo, N. The Challenges of Solar Hybrid PVT Systems in the Food Processing Industry. *Appl. Therm. Eng.* **2021**, *184*, 116235. [\[CrossRef\]](#)
- Imtiaz Hussain, M.; Ali, A.; Lee, G.H. Multi-Module Concentrated Photovoltaic Thermal System Feasibility for Greenhouse Heating: Model Validation and Techno-Economic Analysis. *Sol. Energy* **2016**, *135*, 719–730. [\[CrossRef\]](#)
- Hosouli, S.; Gomes, J.; Loris, A.; Pazmiño, I.-A.; Naidoo, A.; Lennermo, G.; Mohammadi, H. Evaluation of a Solar Photovoltaic Thermal (PVT) System in a Dairy Farm in Germany. *Sol. Energy Adv.* **2023**, *3*, 100035. [\[CrossRef\]](#)
- Kalogirou, S.A. Solar Thermal Collectors and Applications. *Prog. Energy Combust. Sci.* **2004**, *30*, 231–295. [\[CrossRef\]](#)
- Sun, L.L.; Li, M.; Yuan, Y.P.; Cao, X.L.; Lei, B.; Yu, N.Y. Effect of Tilt Angle and Connection Mode of PVT Modules on the Energy Efficiency of a Hot Water System for High-Rise Residential Buildings. *Renew. Energy* **2016**, *93*, 291–301. [\[CrossRef\]](#)
- Kallio, S.; Siroux, M. Energy Analysis and Exergy Optimization of Photovoltaic-Thermal Collector. *Energies* **2020**, *13*, 5106. [\[CrossRef\]](#)
- Rejeb, O.; Dhaou, H.; Jemni, A. A Numerical Investigation of a Photovoltaic Thermal (PV/T) Collector. *Renew. Energy* **2015**, *77*, 43–50. [\[CrossRef\]](#)
- Lämmle, M.; Kroyer, T.; Fortuin, S.; Wiese, M.; Hermann, M. Development and Modelling of Highly-Efficient PVT Collectors with Low-Emissivity Coatings. *Sol. Energy* **2016**, *130*, 161–173. [\[CrossRef\]](#)
- Aste, N.; Del Pero, C.; Leonforte, F.; Manfren, M. Performance Monitoring and Modeling of an Uncovered Photovoltaic-Thermal (PVT) Water Collector. *Sol. Energy* **2016**, *135*, 551–568. [\[CrossRef\]](#)
- Kazem, H.A.; Al-Waeli, A.H.A.; Chaichan, M.T.; Al-Waeli, K.H.; Al-Aasam, A.B.; Sopian, K. Evaluation and Comparison of Different Flow Configurations PVT Systems in Oman: A Numerical and Experimental Investigation. *Sol. Energy* **2020**, *208*, 58–88. [\[CrossRef\]](#)
- Herrando, M.; Ramos, A.; Zabalza, I.; Markides, C.N. A Comprehensive Assessment of Alternative Absorber-Exchanger Designs for Hybrid PVT-Water Collectors. *Appl. Energy* **2019**, *235*, 1583–1602. [\[CrossRef\]](#)
- Nitsas, M.T.; Koronaki, I.P. Experimental and Theoretical Performance Evaluation of Evacuated Tube Collectors under Mediterranean Climate Conditions. *Therm. Sci. Eng. Prog.* **2018**, *8*, 457–469. [\[CrossRef\]](#)
- Korres, D.N.; Tzivanidis, C. A Novel Asymmetric Compound Parabolic Collector under Experimental and Numerical Investigation. *Renew. Energy* **2022**, *199*, 1580–1592. [\[CrossRef\]](#)
- Bernardo, L.R.; Perers, B.; Håkansson, H.; Karlsson, B. Performance Evaluation of Low Concentrating Photovoltaic/Thermal Systems: A Case Study from Sweden. *Sol. Energy* **2011**, *85*, 1499–1510. [\[CrossRef\]](#)
- Karathanassis, I.K.; Papanicolaou, E.; Belessiotis, V.; Bergeles, G.C. Dynamic Simulation and Exergetic Optimization of a Concentrating Photovoltaic/Thermal (CPVT) System. *Renew. Energy* **2019**, *135*, 1035–1047. [\[CrossRef\]](#)
- Rosell, J.I.; Vallverdú, X.; Lechón, M.A.; Ibáñez, M. Design and Simulation of a Low Concentrating Photovoltaic/Thermal System. *Energy Convers. Manag.* **2005**, *46*, 3034–3046. [\[CrossRef\]](#)
- Wang, G.; Wang, B.; Yuan, X.; Lin, J.; Chen, Z. Novel Design and Analysis of a Solar PVT System Using LFR Concentrator and Nano-Fluids Optical Filter. *Case Stud. Therm. Eng.* **2021**, *27*, 101328. [\[CrossRef\]](#)

23. Nilsson, J.; Håkansson, H.; Karlsson, B. Electrical and Thermal Characterization of a PV-CPC Hybrid. *Sol. Energy* **2007**, *81*, 917–928. [[CrossRef](#)]
24. Koronaki, I.P.; Nitsas, M.T. Experimental and Theoretical Performance Investigation of Asymmetric Photovoltaic/Thermal Hybrid Solar Collectors Connected in Series. *Renew. Energy* **2018**, *118*, 654–672. [[CrossRef](#)]
25. Nasserian, P.; Afzali Gorouh, H.; Gomes, J.; Cabral, D.; Salmanzadeh, M.; Lehmann, T.; Hayati, A. Numerical and Experimental Study of an Asymmetric CPC-PVT Solar Collector. *Energies* **2020**, *13*, 1669. [[CrossRef](#)]
26. Guarracino, I.; Mellor, A.; Ekins-Daukes, N.J.; Markides, C.N. Dynamic Coupled Thermal-and-Electrical Modelling of Sheet-and-Tube Hybrid Photovoltaic/Thermal (PVT) Collectors. *Appl. Therm. Eng.* **2016**, *101*, 778–795. [[CrossRef](#)]
27. Korres, D.N.; Bellos, E.; Tzivanidis, C. Integration of a Linear Cavity Receiver in an Asymmetric Compound Parabolic Collector. *Energies* **2022**, *15*, 8635. [[CrossRef](#)]
28. Korres, D.N.; Tzivanidis, C.; Koronaki, I.P.; Nitsas, M.T. Experimental, Numerical and Analytical Investigation of a U-Type Evacuated Tube Collectors' Array. *Renew. Energy* **2019**, *135*, 218–231. [[CrossRef](#)]
29. Çengel, Y.A.; Cimbala, J.M. *Fluid Mechanics: Fundamentals and Applications*, 4th ed.; McGraw-Hill Education: New York, NY, USA, 2018; ISBN 978-1-259-69653-4.
30. Bellos, E.; Korres, D.N.; Tzivanidis, C. Investigation of a Compound Parabolic Collector with a Flat Glazing. *Sustainability* **2023**, *15*, 4347. [[CrossRef](#)]
31. Petela, R. Exergy of Undiluted Thermal Radiation. *Sol. Energy* **2003**, *74*, 469–488. [[CrossRef](#)]
32. Blanco, M.J.; Mutuberría, A.; Garcia, P.; Gastesi, R.; Martin, V. Preliminary Validation of Tonatiuh. In Proceedings of the SolarPACES 2009 International Conference, Berlin, Germany, 15–18 September 2009; Volume 1, p. 2009.
33. Afzali Gorouh, H.; Salmanzadeh, M.; Nasserian, P.; Hayati, A.; Cabral, D.; Gomes, J.; Karlsson, B. Thermal Modelling and Experimental Evaluation of a Novel Concentrating Photovoltaic Thermal Collector (CPVT) with Parabolic Concentrator. *Renew. Energy* **2022**, *181*, 535–553. [[CrossRef](#)]
34. Christodoulaki, R.; Tsekouras, P.; Koronaki, I. On the Optical Performance of a Spherical Stationary Reflector/Tracking Absorber Solar Collector. *Int. J. Sustain. Energy* **2022**, *41*, 1–11. [[CrossRef](#)]
35. *Technical Reference Solidworks Flow Simulation 2015*; Dassault Systems: Vélizy-Villacoublay, France, 2015.
36. *COMSOL Multiphysics Reference Manual*; COMSOL AB: Stockholm, Sweden, 2019.
37. Miao, R.; Hu, X.; Yu, Y.; Zhang, Y.; Wood, M.; Olson, G.; Yang, H. Evaluation of Cooling Performance of a Novel Dual-Purpose Solar Thermal Collector through Numerical Simulations. *Appl. Therm. Eng.* **2022**, *204*, 117966. [[CrossRef](#)]
38. Chandan; Suresh, V.; Iqbal, S.M.; Reddy, K.S.; Pesala, B. 3-D Numerical Modelling and Experimental Investigation of Coupled Photovoltaic Thermal and Flat Plate Collector. *Sol. Energy* **2021**, *224*, 195–209. [[CrossRef](#)]
39. Hassanzadeh, A.; Jiang, L.; Winston, R. Coupled Optical-Thermal Modeling, Design and Experimental Testing of a Novel Medium-Temperature Solar Thermal Collector with Pentagon Absorber. *Sol. Energy* **2018**, *173*, 1248–1261. [[CrossRef](#)]
40. Huld, T.; Müller, R.; Gambardella, A. A New Solar Radiation Database for Estimating PV Performance in Europe and Africa. *Sol. Energy* **2012**, *86*, 1803–1815. [[CrossRef](#)]
41. *Greek Regulation for Buildings Energy Performance, Technical Notes 20701–3/2010*; Technical Chamber of Greece: Athens, Greece, 2010.
42. Korres, D.; Tzivanidis, C. Thermal Analysis of a Serpentine Flat Plate Collector and Investigation of the Flow and Convection Regime. *Therm. Sci.* **2019**, *23*, 47–59. [[CrossRef](#)]

Disclaimer/Publisher's Note: The statements, opinions and data contained in all publications are solely those of the individual author(s) and contributor(s) and not of MDPI and/or the editor(s). MDPI and/or the editor(s) disclaim responsibility for any injury to people or property resulting from any ideas, methods, instructions or products referred to in the content.